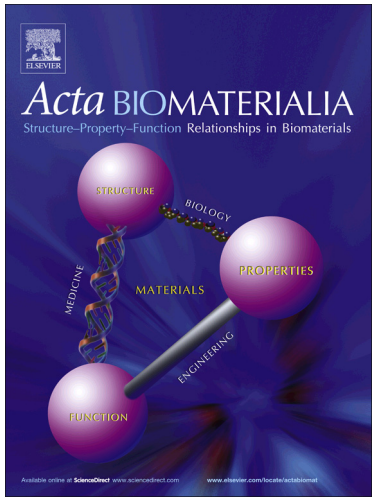

Full length article

In vitro response of mesenchymal stem cells to biomimetic hydroxyapatite substrates: a new strategy to assess the effect of ion exchange

Joanna Maria Sadowska, Jordi Guillem-Marti, Montserrat Espanol, Christoph Stähli, Nicola Döbelin, Maria-Pau Ginebra

PII: S1742-7061(18)30371-4
DOI: https://doi.org/10.1016/j.actbio.2018.06.025
Reference: ACTBIO 5535

To appear in: *Acta Biomaterialia*

Received Date: 10 January 2018
Revised Date: 29 May 2018
Accepted Date: 18 June 2018

Please cite this article as: Maria Sadowska, J., Guillem-Marti, J., Espanol, M., Stähli, C., Döbelin, N., Ginebra, M-P., In vitro response of mesenchymal stem cells to biomimetic hydroxyapatite substrates: a new strategy to assess the effect of ion exchange, *Acta Biomaterialia* (2018), doi: https://doi.org/10.1016/j.actbio.2018.06.025

In vitro response of mesenchymal stem cells to biomimetic hydroxyapatite substrates: a new strategy to assess the effect of ion exchange

Joanna Maria Sadowska[1,2], Jordi Guillem-Marti[1,2], Montserrat Espanol[1,2], Christoph Stähli[3], Nicola Döbelin[3], Maria-Pau Ginebra[1,2,4]

[1]Biomaterials, Biomechanics and Tissue Engineering Group, Department of Materials Science and Metallurgical Engineering, Universitat Politècnica de Catalunya (UPC), Av. Eduard Maristany 16, 08019 Barcelona, Spain.

[2]Barcelona Research Centre in Multiscale Science and Engineering, Universitat Politècnica de Catalunya (UPC), Av. Eduard Maristany 16, 08019 Barcelona, Spain.

[3]RMS Foundation, Bischmattstrasse 12, 2544 Bettlach, Switzerland

[4]Institute for Bioengineering of Catalonia (IBEC), The Barcelona Institute of Science and Technology, Baldiri Reixac 10-12, 08028 Barcelona Spain.

*Corresponding author

Maria-Pau Ginebra Molins

Biomaterials, Biomechanics and Tissue Engineering Department

Department of Materials Science and Metallurgical Engineering

Universitat Politècnica de Catalunya

Avinguda Eduard Maristany 16, 08019, Barcelona, Spain

Tel: +34 934017706

Email: maria.pau.ginebra@upc.edu

ABSTRACT

Biomaterials can interact with cells directly, that is, by direct contact of the cells with the material surface, or indirectly, through soluble species that can be released to or uptaken from the surrounding fluids. However, it is difficult to characterise the relevance of this fluid-mediated interaction separately from the topography and composition of the substrate, because they are coupled variables. These fluid-mediated interactions are amplified in the case of highly reactive CaPs such as biomimetic calcium deficient hydroxyapatite (CDHA), particularly in static in vitro cultures. The present work proposes a strategy to decouple the effect of ion exchange from topographical features by adjusting the volume ratio between the cell culture medium and biomaterial (V_{CM}/V_B). Increasing this ratio allowed mitigating the drastic ionic exchanges associated to the compositional changes experienced by the material exposed to the cell culture medium. This strategy was validated using rat mesenchymal stem cells (rMSCs) cultured on CDHA and beta-tricalcium phosphate (β-TCP) discs using different (V_{CM}/V_B) ratios. Whereas in the case of β-TCP the cell response was not affected by this ratio, a significant effect on cell adhesion and proliferation was found for the more reactive CDHA. The ionic exchange, produced by CDHA at low $V_{CM}/V_{B,}$ altered cell adhesion due to the reduced number of focal adhesions, caused cell shrinkage and further rMCSs apoptosis. This was mitigated when using a high V_{CM}/V_B, which attenuated the changes of calcium and phosphate concentrations in the cell culture medium, resulting in rMSCs spreading and a viability over time. Moreover, rMSCs showed an earlier expression of osteogenic genes on CDHA compared to sintered β-TCP when extracellular calcium fluctuations were reduced.

Statement of significance

Fluid mediated interactions play a significant role in the bioactivity of calcium phosphates. Ionic exchange is amplified in the case of biomimetic hydroxyapatite, which makes the in vitro characterisation of cell-material interactions especially challenging. The present work proposes a novel and simple strategy to explore the mechanisms of interaction of biomimetic and sintered calcium phosphates with mesenchymal stem cells. The effects of topography and ion exchange are analysed separately by modifying the volume ratio between cell culture medium and biomaterial. High ionic fluctuations interfered in the maturation of focal adhesions, hampering cell adhesion and leading to increased apoptosis and reduced proliferation rate.

Keywords: calcium phosphates, mesenchymal stem cells, intracellular calcium, cell adhesion

1. INTRODUCTION

Calcium phosphates are increasingly used as bone graft substitutes due to their similarity to the mineral phase of bone and their osteogenic potential. However, although some advances have been made in the last years, the design of synthetic bone grafts that outperform autografts remains an open challenge. For this to be possible, it would be necessary to have a more systematic knowledge of the effect of the different material properties on the biological response [1].

Topography and textural properties, like the micro/nanostructure or porosity have been shown to influence the biological performance of calcium phosphates both in vitro and in vivo, affecting for instance the bioactivity, osteogenic and osteoinductive properties [2–6]. This has been often attributed to the sensitivity of adherent cells to the topography of the substrate. Whereas this can be a straightforward conclusion for bioinert substrates, the situation in the case of bioactive materials like CaPs is far more complex. In addition to the direct contact effects, materials can influence cell behaviour indirectly, through fluid-mediated effects, that is, through the interaction with the body fluids where the cells are immersed. For instance, it is well accepted that, amongst the parameters that contribute to the excellent performance of calcium phosphates as bone substitute materials, the ionic exchange promotes the creation of a favourable microenvironment leading to bone formation [1,7–11].

The complexity arises because topography and ionic exchange are strictly coupled variables. The ionic exchange between material and the surrounding fluid is dependent on both the chemical composition and the microstructure or topography of the material. For a given chemical composition, the ionic exchange with the surrounding medium will be modified if the materials' topography, and consequently the specific surface area is modified. Hence, the difficulty to analyse these two parameters independently, and the risk to wrongly attribute to topography an effect that in reality can be chemical, *i.e.*, associated to the modification of the soluble ions present in solution, which come into contact with the cells.

The identification of the individual effects of topography and ionic exchange is particularly relevant in the *in vitro* studies where, due to the specific conditions, some materials, especially those having high specific surface areas, can induce considerable ionic exchange in the cell culture medium [12,13]. In these cases, the interpretation of the results and the extrapolation to the in vivo scenario, where continuous fluid renewal occurs, becomes especially challenging [14].

The synthesis routes using biomimetic conditions, based on precipitation reactions at body temperature, allow obtaining bulk calcium phosphate materials that are much closer to the mineral phase of bone than sintered calcium phosphate ceramics. For instance, the hydrolysis of alpha-tricalcium phosphate (α-TCP) at body temperature results in nanometric crystals of hydroxyapatite which, like the mineral phase of bone is calcium deficient, contains HPO_4^{-2} groups, has low crystallinity and high specific surface area [15] For all these reasons it is referred to as biomimetic calcium deficient hydroxyapatite.

In previous works we demonstrated that sintered ceramics and biomimetic calcium deficient hydroxyapatite (CDHA, $Ca_9(HPO_4)(PO_4)_5(OH)$) altered the ionic composition of the cell culture media to different extents, affecting the behaviour of osteoblastic and mesenchymal stem cells [16]. This was especially striking in the case of biomimetic CDHA, a material that while having an excellent *in vivo* response, with superior osteogenic and osteoinductive properties [17],

drastically impaired the viability of rat mesenchymal stem cells (rMSCs). This effect was confirmed by seeding the cells either in direct contact with the surface of CDHA discs or on glass coverslips on top of the CDHA substrates. The results demonstrated that rMSCs were highly sensitive to the ionic fluctuations caused by the biomaterial in the cell culture medium, reaching cytotoxic levels that prevented to study further the cell-material interactions [16]. Paradoxically, the same particular topographical and chemical features of these materials responsible for the excellent in vivo response, namely, its nanostructure, large specific surface area (SSA), deficiency in calcium and low crystallinity caused this poor *in vitro* response [16]. Whereas a further understanding of the specific mechanisms governing the cell-material interaction would be of great interest in view of designing enhanced synthetic bone grafts, the mutual interdependence between nanostructure and ionic exchange hampered the identification of the individual roles of these parameters.

In the present work we proposed a new strategy to overcome the poor *in vitro* results usually obtained with highly reactive biomimetic CDHA, and to discern the role of ionic exchange and topographical features in the response of rMSCs. The strategy consisted in establishing culture conditions that, within the limitations of the static cultures, mimicked better the *in vivo* situation. This was done by adjusting the volume ratio between cell culture medium and biomaterial (V_{CM}/V_B). Thus, cells were cultured either at low ($V_{CM}/V_B \sim 5$) or at high ($V_{CM}/V_B \sim 300$) volume ratios, which exposed them to the same surface chemistry and topography but to different ionic concentrations. We further analysed the effect of the ionic environment on the intracellular free cytoplasmic calcium content and the subsequent processes related to it, such as the adhesion mechanisms, apoptosis and the osteogenic differentiation of rMSCs. β-tricalcium phosphate (β-TCP) was used as a control, as this sintered ceramic is directly obtained by thermal treatment of CDHA, this assuring the same elemental composition and minimising possible interferences from different reagents.

2. MATERIALS AND METHODS

2.1. Material preparation

The synthesis of biomimetic CDHA and β- TCP was described elsewhere [15,16]. Briefly, CDHA was obtained through a cementitious reaction involving the hydrolysis of α-TCP. The solid phase, consisting of α-TCP powder with a 2 wt% of precipitated hydroxyapatite (Merck 2143; Merck, Darmstardt, Germany) was mixed with the help of a spatula with a liquid phase consisting of 2.5 wt% disodium hydrogen phosphate (Na_2HPO_4; Panreac) at a 0.40 mL/g liquid to powder ratio. The paste was then transferred to Teflon moulds. Subsequently, the discs were immersed in water at 37 °C for 7 days to allow for the complete hydrolysis reaction of α-TCP to CDHA to take place. Two dimensions of discs were prepared: i) Large discs: 15 mm Ø x 2 mm height (CDHA-L); and ii) Small discs: 5.5 mm Ø x 0.30 mm height (CDHA-S) (Figure 1B). The β-TCP-L and β-TCP-S discs were obtained by sintering the CDHA-L and CDHA-S discs respectively at 1100 °C during 15 h.

2.2. Material characterisation

The surface microstructure was characterised by scanning electron microscopy (SEM, Zeiss Neon 40) with an acceleration voltage of 5 kV after coating the surface with gold-palladium sputtering with EMITECH K950X. The surface roughness was characterized by optical interferometry (Wyko NT1100; Veeco Instruments, USA), using a 50x magnification and a scanned area of 47.5 x 63.4 μm2. Images were acquired using Vision32 software (Veeco Instruments).

2.3. Cell culture study

Rat mesenchymal stem cells (rMSCs) were isolated from the tibias and femurs of young Lewis rats (2-4 weeks old) and expanded in Advanced Dulbecco's Modified Eagle's Medium (advDMEM) supplemented with 10% foetal bovine serum (FBS), 2 mM L-glutamine, penicillin/streptomycin (50 U/ml and 50 μg/ml, respectively) and 20 mM HEPES, all from Invitrogen (complete advDMEM). HEPES was used as pH buffer to prevent the acidification of the medium by CDHA [12]. For all the experiments, rMSCs at passage 3 and 4 were seeded at a density of 300 cells/mm^2 except where otherwise stated. For cell culture assays, 2 mL of

complete advDMEM medium were used, giving rise to two cell culture conditions: i) low volume ratio between culture medium and biomaterial (V_{CM}/V_B ~ 5), when large discs were used (CDHA-L or β-TCP-L); and ii) high volume ratio between culture medium and biomaterial (V_{CM}/V_B ~ 300) for the small discs (CDHA-S or β-TCP-S) (Fig. 1B).

2.3.1. Initial cell attachment and proliferation

The discs were sterilized by immersion in 70% ethanol and subsequently rinsed thrice with PBS. Afterwards, the discs were placed in 24- well plate and incubated overnight with complete advDMEM. Cells were seeded and after the initial cell attachment (6 hours) samples were transferred to new 24- well plate to discard attached cells at the bottom of well- plate in the small discs. Subsequently, rMSCs were incubated with samples for 6 hours, 3 days, 7 days and 14 days, renewing the medium every day. Tissue culture polystyrene (TCPS) was used as control. At each specified time point, discs were transferred to new 24-well plate, washed thrice with PBS and lysed with 300 µl M-PER® (Mammalian Protein Extraction Reagent, Thermo Scientific, Waltham, MA, USA). Cell number was quantified by Cytotoxicity Detection Kit (Roche Applied Science, Penzberg, Germany) following the manufacturer's protocol. A calibration curve with increasing numbers of cells was prepared. LDH activity was evaluated at 492 nm with Synergy HTX multi-mode microplate reader (Bio-Tek). Results of cell number detected by LDH activity were normalized versus the area of the corresponding substrate. Two independent runs of experiment were performed.

2.3.2. Scanning electron microscopy

Cell morphology was evaluated by scanning electron microscopy (SEM, Zeiss Neon 40) with an acceleration voltage of 5 kV. After placing the discs in new 24- well plate, three rinses with PBS were performed and cells were fixed in 2.5% glutaraldehyde solution in PBS. Afterwards, discs were incubated for 1 h at 4^0C and subsequently washed in PBS (x3) and dehydrated in 50, 70, 90, 96 and 100 % ethanol series. Dehydration process was completed by adding hexamethyldisilazane (HMDS). A thin layer of gold- palladium was deposited on discs by

vapour deposition (EMITECH K950X). Image analysis with Fiji/Image-J package was performed in order to quantify spreading area and aspect ratio of rMSCs over cell culture (n=15).

2.3.3.Measurement of pH, Ca^{2+} and P_i concentration in the cell culture medium

For the evaluation of calcium and phosphate concentrations, at each specified time point, the supernatants *i.e.* the cell culture medium in contact with the CaP substrates were collected. Then, Ca^{2+} content was quantified through calcium o- cresolphthalein complexone method [18,19] whereas P_i through Phosphate Colorimetric Assay Kit (Sigma- Aldrich) following the manufacturer's instructions. The results were measured spectrophotometrically by Synergy HTX multi-mode microplate reader (Bio-Tek) at 570 nm and 650 nm for Ca^{2+} and P_i, respectively. The pH measurements were performed using a selective electrode (CRISON INSTRUMENTS, MultiMeter MM 41). The experiments were performed in two independent runs.

2.3.4.Evolution of the CDHA exposed to FBS-free advDMEM

To analyse the effect of prolonged exposure of CDHA to cell culture medium, CDHA-L and CDHA-S discs were sterilised with 70% ethanol, rinsed thrice with double distilled water (dd H_2O) and incubated overnight with 2 mL of advDMEM without FBS supplementation (FBS was not included to avoid the contribution of the ions bound to proteins as they could interfere upon protein adsorption on the material). The medium renewal was performed every day up to 21 days of incubation. Before incubation, as well as after 14 and 21 days, the discs were broken into two halves and one of them was milled in an agate mortar. The remaining half discs and the powders were then washed three times with dd H_2O and allowed to dry at 37 ^{o}C. To determine the superficial changes in composition, the surface of CDHA-L discs was scraped with a scalpel and the powder was analysed by Fourier transform infrared spectroscopy in the attenuated total reflection mode (ATR-FTIR, Nicolet 6700). Data was acquired in 64 scans with a resolution of 4cm-1 from 4000 to 675cm^{-1} with a Germanium crystal.

The Ca/P ratio was measured from the milled CDHA halves by inductive coupled plasma - mass spectroscopy (ICP-MS; Agilent 7700x, Agilent Technologies, Japan). The powders were dissolved in 69% HNO_3 (w/w) (HNO_3, TraceSELECT®, Sigma Aldrich, Switzerland) and diluted 1:1000 in a solution of demineralized H_2O containing 3% HNO_3, 2% HCl (HCl, Rotipuran® Supra, Carl Roth, Switzerland) and 0.01% HF (HF, TraceSELECT® Ultra, Sigma Aldrich, Switzerland). The solutions were analyzed using ICP-MS. ^{44}Ca and ^{31}P signals were calibrated against a custom-made certified standard solution containing Ca and P ions in a molar ratio of 1.55, and ^{23}Na, ^{25}Mg and ^{88}Sr signals were calibrated against a multi-element standard solution (both: Inorganic Ventures, USA). Calibration drifts were corrected according to the Ca-P standard measured after every 8th sample and according to a 20 ppb internal Sc standard solution (Inorganic Ventures, USA) measured along with each sample. Finally, the mean values of four measurements per sample were determined.

2.3.5.Measurement of intracellular Ca^{2+}

To analyse potential effects of the extracellular calcium fluctuations on the intracellular calcium, this parameter was measured for the cells cultured on CDHA, the substrate that induced higher changes of calcium concentration following the two culture conditions. Cells were seeded on CDHA-L and CDHA-S as described above (Initial cell attachment and proliferation section). After 6 hours of adhesion, samples were transferred to new 24-well plate and adherent cells were detached with trypsin. Both trypsinised cells and supernatants were centrifuged at 300 x g for 5 min. Afterwards, cells were incubated with 5 µM Fluo-4-acetoxymethyl ester, a dye which binds to free cytoplasmic calcium of living cells, (Fluo-4 AM; Molecular Probes) in FBS-free advDMEM for 20 min at 37^0C. Subsequently, cells were centrifuged and resuspended in PBS. The fluorescence emission at 530 nm was measured by a Gallios Flow Cytometer (Beckman Coulter, Brea, CA, USA). A total of 5000 events were evaluated. Afterwards, the flow cytometry data was plotted as forward scatter versus side scatter and gate was determined manually using the unstained rMSCs and rMSCs stained with Fluo-4

AM as a controls. The dead and fragmented cells were excluded from analysis. Summit 4.3 and FlowJo Softwares were used for sample analysis.

2.3.6. Apoptosis/necrosis assays

After 6 hours of adhesion of rMSCs to CDHA-L and CDHA-S, cells were detached as above described (Measurements of intracellular Ca^{2+}), centrifuged and the cell pellet was resuspended using cold PBS. Subsequently, rMSCs were stained with Alexa Fluor 488 Annexin V and Propidium Iodide (PI) using the Dead Cell Apoptosis Kit (Invitrogen) and following manufacturer protocol. TCPS was used as control. The samples were stored on ice till analysis. A total of 5000 events for each condition were analysed by a Gallios Flow Cytometer (Beckman Coulter, Brea, CA, USA) measuring the fluorescence emission at 530 nm (FL1) and >575 nm (FL4) for annexin V and PI staining, respectively. Summit 4.3 Software was used for sample analysis.

Additionally, apoptosis/necrosis pathway on CDHA-L and CDHA-S samples was analysed by visualization in confocal microscopy. For that purpose, CDHA-L and CDHA-S were washed with cold PBS and stained with Dead Cell Apoptosis Kit. Afterward, cells were fixed with 4% paraformaldehyde (PFA) solution in PBS. For nuclei visualisation, discs were incubated with 4',6-diamidino-2-phenylindole (DAPI, 1:1000 in 0.15% glycine in PBS) for 2 minutes. Cells seeded on glass coverslip were used as a control. Samples were visualized in a TCS SPE confocal microscope (Leica Microsystems). Images were acquired using the LASX software and processed using Fiji/Image-J package.

2.3.7. Immunofluorescence staining

Cell morphology and adhesion on CDHA-L and CDHA-S was investigated by staining of cytoskeleton, focal adhesions and fibronectin (FN) secretion. rMScs seeded on glass coverslip were used as a control. The study was performed at 6 hours, and 1, 2 and 3 days of cell culture. Attached cells were rinsed with PBS (x3) and fixed in 4% PFA solution in PBS. Afterwards, cells were permeabilized with 300 µL of 0.1 % Triton X- 100 (Sigma-Aldrich) in PBS for 15

minutes and blocked with 1% bovine serum albumin (BSA) (Sigma-Aldrich) in PBS for 30 min. Then, the discs were incubated for 1 hour with the following primary antibodies: mouse anti-vinculin (sigma-Aldrich), rabbit anti- fibronectin (Sigma-Aldrich) or rabbit anti- phospho-FAK (pFAK; pTyr397 specific, Santa Cruz Biotechnologies), all at 1:100 in 1% BSA in PBS. Afterwards, appropriate secondary antibodies were added: Alexa Fluor 488 goat anti- mouse (1:1000) or Alexa Fluor 488 goat anti-rabbit (1:1000) were incubated with Alexa Fluor 546 Phalloidin (1:300) for 1 hour in 0.1% Triton X- 100 in PBS (all from Invitrogen). For nuclei staining, the discs were incubated with DAPI (1:1000 in 0.15% glycine in PBS) for 2 minutes. Between all steps, three rinses for 5 minutes with 0.15% glycine (Sigma-Aldrich) in PBS were performed. Discs were mounted with Mowiol 4-88 (Sigma-Aldrich) and visualized using a TCS SPE confocal microscope (Leica Microsystems, Germany). Cells seeded on glass coverslip were used as a control. Images were acquired using LASX software and processed using Fiji/Image-J package. Additionally, image analysis was performed in order to quantify the evolution of spreading area and aspect ratio (n=15) on CDHA discs at short time points. The pFAK area (n=10) was measured at day 3 of cell culture.

2.3.8. Gene expression

The differentiation of rMSCs to osteoblastic phenotype was assessed on CDHA-S and β- TCP-S by measuring gene expression of osteoblastic markers by real time quantitative polymerase chain reaction (qRT-PCR). Total RNA was extracted at 6 hours, 1 day and 3 days using RNeasy® Mini Kit (Qiagen, Hilden, Germany) and following manufacturer instructions. Samples were previously transferred to new 24-well plates and rinsed thrice in PBS. Subsequently, total RNA was quantified by NanoDrop ND-1000 spectrophotometer (NanoDrop Technologies, Montchanin, DE, USA) and 150 ng of RNA were used for synthesis of complementary DNA (cDNA) using the QuantiTect Reverse Transcription Kit (Qiagen). cDNA templates were amplified using the QuantiTect SYBR Green RT-PCR Kit (Qiagen) in a StepOnePlus Real-Time PCR System (Applied Biosystems, Foster City, CA, USA) using specific primers for osteoblastic markers (Table 1). In all RT-qPCR runs, specificity of primers

was determined by melt curves analysis. Moreover, negative controls *i.e.* no- RNA control and no- RT control were run in parallel in order to ensure that contamination and genomic DNA were not present. The values were normalised by expression of reference gene *i.e.* β-actin (ACTB) and relative fold changes (FC) were related to TCPS at 6h of culture using the following Equation 1 [20].

$$FC = \frac{\text{Etarget}^{\Delta \text{Cq target (TCPS 6h - sample)}}}{\text{Ereference}^{\Delta \text{Cq target (TCPS 6h-sample)}}} \quad (1)$$

Cq respresents the median value of the quantification cycle of the triplicate of each sample. E corresponds to the efficiency of amplification and is determined through following formula $E = 10^{[-1/\text{slope}]}$ where slope value proceeds from slope of the log-linear portion of the calibration-curve. The experiment was performed in three independent runs. No osteogenic medium was used for CDHA- S and β- TCP-S except for the evaluation of OCN gene expression, where osteogenic medium (OM) containing 50 µm/ mL ascorbic acid, 10 mM β- glycerophosphate and 100 nM dexamethasone in complete medium was used. The osteogenic medium was added 6 hours after cell seeding.

Table 1. DNA sequences of forward and reverse primers used for the RT-qPCR.

Gene title	**Gene symbol**	**Forward primer sequence (5'→3')**	**Reverse primer sequence (5'→3')**
β-actin	ACTB	CGTCATCCATGGCGA ACT	CCCGCGAGTACAACCTTCT
Alkaline phosphatase	ALP	TCAGTTCTGTTCTTGGGGTA CAT	GCACAACATCAAGGACATCG
Bone morphogenic protein-2	BMP-2	CCCCTATATGCTCGACCT CT	AAAGTTCCTCGATGGCTTCTT
Collagen I	COLLI	CATGTTCAGCTTTGTGGAC CT	GCAGCTGACTTCAGGGATGT
Osteocalcin	OCN	CCAGGGGATCTGGGTAGG	ATAGACTCCGGCGCTACCTC
Osteonectin	ONN	GGTTCTGGCAGGGGTTTT	GTTTGAAGAAGGTGCAGAGG A
Osteopontin	OPN	GGCTACAGCATCTGAGTGT TTG	CGGTGAAAGTGGCTGAGTTT

2.4. Statistical analysis

The experiments were performed in triplicate, with three independent runs in each test, except where otherwise stated. The results are presented as mean ± standard error. Statistical analysis for parametric data (the results of flow cytometry) was performed using T- Student test. For non- parametric data, Kruskal-Wallis test was applied, followed by multiple pairwise comparison. Significance level was set as p-value < 0.05.

3. RESULTS

3.1. Material characterisation

SEM micrographs revealed that the topography of CDHA consisted of aggregates of plate-like crystals, whilst the sintering process led to a polyhedral grain structure for β-TCP. The average roughness was higher for CDHA (Sa=2.53 ±0.72 μm) compared to β-TCP (Sa=1.33±0.23 μm) (Figure 1A). The XRD results showed that both substrates were phase-pure, with all peaks matching those in JCPDS 82-1943 (HA) and JCPDS 70- 2065 (β-TCP) for CDHA and β-TCP, respectively (Supplementary Figure 1). Due to the low crystallinity of the CDHA phase, the XRD pattern of biomimetic CDHA showed wider peaks compared to sintered β-TCP. Further physicochemical characterisation of both CaP materials can be found in a previous work [16].

3.2. Initial cell adhesion and proliferation

Cell proliferation was slower in the four CaP substrates than in TCPS, and in general cell number was larger in β-TCP than in CDHA. Interestingly, different trends were found in relation to the effect of V_{CM}/V_B on cell proliferation when comparing CDHA and β-TCP. Whereas cell number increased with time on β-TCP irrespective of the V_{CM}/V_B used, on the CDHA cell proliferation was significantly affected by the V_{CM}/V_B (Figure 2A). When cells were cultured on the large CDHA discs (CDHA-L) cell number decreased over time. In contrast, this tendency was reversed and a slow increase in cell number was observed when cells were cultured on the small discs (CDHA-S), although the values reached were significantly lower than those observed for β-TCP and TCPS.

3.3. Interactions between the CDHA substrates and the cell culture medium

The evolution of extracellular Ca^{2+} and P_i over time in presence of cells is displayed in Figure 2B. The experimental value of Ca^{2+} in complete advDMEM cell culture medium was 1.78 ± 0.17 mM. Different trends were found in relation to the effect of V_{CM}/V_B when comparing CDHA and β-TCP. Whereas the Ca^{2+} concentration in the culture medium was unaltered in contact with β-TCP discs, irrespective of its size, a significant decrease of calcium concentration was produced in contact with the CDHA-L discs, which did not happen for the small CDHA discs. After 6 hours, the Ca^{2+} concentration decreased approximately 25% of the initial experimental value and continued decreasing up to 40% at days 3 and 7. At day 14 the calcium concentration increased slightly, reaching similar values to those at 6 hours, which reflected that the uptake of Ca was slowly becoming saturated.

Small changes of P_i concentration in the cell culture medium were observed for all the substrates, the concentration remaining closer to the initial value (1.17 ± 0.10 mM) (Figure 2B, middle panel). Little variation was observed in the pH of the cell culture medium throughout the cell culture study in all CaP discs (Figure 2B, bottom panel).

Regarding the CDHA substrates, no changes were observed by SEM in the microstructure of the surface of the discs after exposure to FBS- free advDMEM for 21 days. Both CDHA-L and CDHA-S exhibited the typical plate- like crystal morphology already revealed on the pristine substrates (Supplementary Figure 2). Interestingly, FTIR analysis of the surface of the discs revealed the presence of carbonate bands on CDHA-L samples exposed to the cell culture medium (Figure 2C, right panel). The bands at 1471 and 1419 cm^{-1} can be ascribed to a B-type substituted apatite whilst the one observed at 874 cm^{-1} can be assigned to either $HPO4^{2-}$ or to a B-type carbonate substituted apatite [21–25].. The remaining bands at 964 and 1030 cm^{-1} correspond to typical vibrational modes of phosphate in apatite [26]. The modification of the discs surface chemistry was further confirmed through X-ray photoelectron spectroscopy (XPS) (Supplementary Figures 3A and 3B). In addition, ICP-MS analyses performed after dissolution of powdered discs led to an increase in the Ca/P ratio of 0.90 ± 0.13% and 1.67 ± 0.24% for

CDHA-L and CDHA-S at 14 day, respectively (Figure 2C, left panel). It is worth stressing that these values are an average of the whole volume of the samples, and do not to correspond to the surface. There were no significant changes in Ca/P ratio between 14 and 21 day of incubation. Similar trends were observed for the Mg/P and Na/P ratios (Supplementary Figure 4).

3.4. Cell morphology

The micrographs of the morphological studies performed by SEM are shown in Figure 3. Cells were well adhered after 6 hours, presenting similar flattened morphology in all CaPs. Nonetheless, after 3 days of culture rMSCs exhibited differences in shape depending on the substrate. In both β- TCP-L and β- TCP-S, rMSCs maintained their initial flattened and spread morphology showing similar cell spreading area as well as aspect ratio (Figures 3 B and C). In contrast, on CDHA-S the rMSCs became more spindle-shaped, with a higher aspect ratio compared to the initial time point (Fig. 3C). The most remarkable changes occurred for the low V_{CM}/V_B ratio, that is, for CDHA-L discs. In this case, although rMSCs showed flattened morphology at 6 hours a progressive decrease in cell spreading was observed over time, together with a reduction in cell number (Figures 3A and B). Moreover, the cells cultured on CDHA-L presented a significantly lower aspect ratio compared to CDHA-S, remaining round-shaped throughout the cell culture (Figure 3C).

3.5. Free-intracellular calcium

The free-intracellular calcium for the cells cultured on CDHA is displayed in Figure 4. The dead and fragmented cells were excluded from the analysis and the fluorescence was normalized by cell size [27,28]. Thus, the values of median fluorescence of Fluo-4 represent the levels of intracellular calcium of viable, gated cells (Figure 4A, coloured dots). A shift of fluorescence emission of Fluo-4 was observed when rMSCs were cultured on CDHA-L and CDHA-S compared to TCPS (Figure 4B). The results showed a no statistically significant decrease of 4.86± 21.01% of median fluorescence of Fluo-4 for CDHA- L (Median=0.067± 0.01) compared to TCPS (Median= 0.0705± 0.00). In contrast, the Fluo-4 fluorescence levels for CDHA-S

(Median=0.11± 0.02) were 61.87± 33.72% higher than the TCPS values (Figure 4D). The experiment was performed in four independent runs.

3.6. Cell death pathway

The pathway of rMSCs death was evaluated for CDHA-L and CDHA-S discs (Figure 5) and represented as a contour diagram of Anexin V Alexa Fluor 488/ PI intensity staining. The viable cells appear negatively stained for PI and Alexa Fluor 488- Annexin V and are represented at left lower quadrant. The positively stained cells for Alexa Fluor 488- Annexin V and negatively stained for PI are considered apoptotic cells and are represented in the right lower quadrant. The left upper quadrant represents necrotic cells that positive stain for PI but are negative for Alexa Fluor 488- Annexin V. Late apoptotic cells display binding for both PI and Alexa Fluor 488- Annexin V and are represented in the right upper quadrant. The percentage of viable was significantly reduced for CDHA-L (65.20%) compared to the control, and non-viable cells were mainly late apoptotic cells (21.64%), although there was also a percentage of apoptotic and necrotic cells (6.6 and 6.56% respectively). The percentage of viable cells increased when the ratio V_{CM}/V_B increased. Thus, when the small discs were used (CDHA-S), the percentage of viable cells was 82.58%, with 8.53% of late apoptotic cells, 7.88% of apoptotic cells and very few necrotic cells. The results were confirmed through the visualisation by confocal microscope (Figures 5D-I)).

3.7. Immunofluorescence staining

The morphology of rMSCs on CDHA-L and CDHA-S was studied by immunofluorescence, staining the nuclei, the actin cytoskeleton and either FN (Figure 6) or pFAK (Figure 7). The formation of actin stress fibers was delayed in cells cultured on CDHA compared to TCPS. Noteworthy, V_{CM}/V_B had a strong effect on the cytoskeletal organisation, the cells cultured on CDHA-S presenting a well-defined cytoskeletal organization after 1 day of culture whilst non-maturation of actin stress fibers was observed on CDHA-L throughout the analysed time points (Figures 6 and 7). A reduced staining of both FN and pFAK was observed in both CDHA substrates compared to TCPS (Figures 6 and 7A). Again, strong differences were found when

the V_{CM}/V_B ratio was modified, as whereas in CDHA-S fibronectin production and focal adhesions were clearly observed, they were hardly visible in CDHA-L (Figures 6 and 7A and D). Moreover, CDHA-L resulted in a significant reduction of cell area after 6h. This trend, instead, was not observed for CDHA-S, where a progressive cell spreading was observed (Figure 7A and B).

3.8. Gene expression

The expression of osteoblastic specific markers by rMSCs cultured on the CDHA and β-TCP small discs was performed using RT-qPCR (Figure 8). It was not possible to measure them in large discs due to small cell numbers. An increase in the ALP and collagen I gene expression was observed on CDHA-S at 6h compared to sintered β-TCP-S (1.78±0.31 and 1.18±0.12- fold up- regulation, respectively). However, the expression of both genes decreased progressively over time on both CDHA-S and β-TCP-S, more markedly for CDHA-S. The expression of late osteogenic markers *i.e.* ONN and OPN was similar on both CDHA-S and β-TCP-S at 6 h. However, CDHA-S showed an up-regulation of both ONN and OPN at 1 day. The relative expression level of ONN and OPN on CDHA-S compared to β-TCP-S was 2.15±0.52 and 1.52±0.44, respectively. Since no expression of OCN was detected at short- term cell culture on CDHA-S, the study was performed replacing basic cell culture medium for osteogenic medium after cell adhesion (6h). The results for the expression of OCN were similar to those of ONN gene. Whereas at 6h the expression levels of OCN were lower on CDHA-S than on β-TCP-S (*i.e.*0.21±0.17-fold lower), a 2.59±1.02-fold up-regulation was observed at day 1 on CDHA-S compared to β-TCP-S. Finally, the expression levels of BMP-2 were higher for CDHA-S at all time points, and more markedly at 6h (3.92±0.66- fold compared to β-TCP-S), although they decreased over time.

4. DISCUSSION

Ionic exchange is believed to be one of the mechanisms that play a crucial role in the processes of bone regeneration induced by calcium phosphate biomaterials. Once implanted in the host

bone, the degradation of CaPs, mostly mediated by the action of osteoclastic cells, result in the alteration of the ionic concentrations, mainly calcium and phosphate, in the surrounding extracellular fluids. It is generally accepted that both ions, either alone or simultaneously, foster the process of bone formation, by enhancing the activity of bone-forming cells, but also triggering the differentiation of mesenchymal stem cells to the osteogenic lineage [9,10,29–31].

The extent of this ionic exchange depends on the intrinsic biomaterial properties. For instance, in the case of biomimetic calcium deficient hydroxyapatite, the deficiency in calcium, low crystallinity and SSA lead to a highly reactive material, which can be even more soluble than sintered β-TCP [32] and displays a high bioactivity and osteoinductive properties [17]. These features, which are highly beneficial in the *in vivo* scenario, may however introduce a high level of complexity when looking at the *in vitro* cell response to these materials. The interaction of CDHA with the cell culture medium can cause ionic exchanges that may be detrimental *in vitro*, where cells are cultured in a limited amount of medium, which is periodically renewed. Recently, we demonstrated that CDHA was cytotoxic for rMSCs. However, the specific mechanisms were unknown [16].

The results obtained in the present study highlight that, unlike in other less reactive CaPs, the outcome of the *in vitro* cell response of biomimetic CDHA is strongly influenced by the ionic exchange with the surrounding medium, which in turn is dependent on cell culture conditions. Specifically, changing the volume ratio between cell culture medium and biomaterial from a low ratio (~5) to a high ratio (~300) allowed to show separately the effect of the ionic concentration on the cells cultured on substrates with the same chemistry and topography. A significant effect of V_{CM}/V_B was revealed on the proliferation of rMSCs cultured on CDHA, while the differences were irrelevant for the cells cultured on β-TCP (Figure 2A). Indeed, rMSCs adhered and proliferated well on β-TCP-L and β-TCP-S over time consistent with other reported works [33,34].This different behaviour between materials could be clearly correlated with the changes of Ca^{2+} content in the cell culture medium (Figure 2B).The reduction in cell number on the CDHA-L should be attributed to the high decrease of extracellular Ca^{2+}, which

was prevented increasing the V_{CM}/V_B, that is, choosing *in vitro* conditions that are closer to the physiological situation (Figure 2B). In contrast, the values of Ca^{2+} and P_i for β-TCP discs remained similar to those of TCPS independently of sample dimensions. Despite β-TCP being more soluble than CDHA, its low SSA resulted in a smaller ionic exchange with the culture medium [32]. Accordingly, cell proliferation was not affected by the dimensions of the specimens (Figure 2A). The still lower proliferation on CDHA-S compared to β-TCP and TCPS might be attributed to the surface chemistry or the topographical features of CDHA as previously reported [16].

According to these results, a more appropriate evaluation of the cytotoxicity of highly reactive materials like high SSA CDHA should consider using larger cell culture medium volumes to attenuate the effects of strong ionic changes in the cell culture medium. However, this strategy would still have some drawbacks, as it would overlook the potential cytotoxicity associated to undesirable ions/components that could leach out in the case of materials containing toxic contaminants.

The values of calcium and phosphate concentration (Figure 2B) must be analysed with care, since they represent average supernatant concentrations. The reactivity of the CaP triggers the uptake and release of ions by the material, this creating a gradient of ionic concentrations in the surrounding fluid. Therefore, in static conditions the local content of calcium and phosphate in the close proximity of the cells, that is, in the cell-material interphase, might differ from the average measured in the supernatant. ICP and FTIR analyses of the material after soaking in serum-free and cell-free culture conditions proved changes in the composition of CDHA without alteration of the plate-like microstructure. The ICP measurements showed an increase in the average Ca/P ratio, more pronounced in small than in large discs. This in fact indicates that the Ca/P changes are taking place progressively from the surface of the specimens, which is in contact with the cell culture medium. The larger surface to volume ratio of the small discs explains the higher average Ca/P values in the small than in the large discs. ICP also revealed the incorporation of other ions from the cell culture medium such as Na and Mg. The increase of

the Ca/P would be consistent with the uptake of calcium from the solution, which is known to be associated to the maturation of CDHA ($Ca_9(HPO_4)(PO_4)_5OH$) to a more stoichiometric HA ($Ca_{10}(PO_4)_6(OH)_2$). However, since carbonate gets also incorporated into the apatite lattice substituting phosphate groups (B-type substitution, Fig.2C), this raises also the Ca/P, making it difficult to distinguish the calcium uptake due to maturation from the carbonation process. One aspect worth noting in the cell culture assay was the raise in Ca concentration between 7 and 14d of immersion of the CDHA-L discs (Fig. 2B), pointing that the effect of CDHA in the environment was being attenuated. The duration of this transient effect might depend on the conditions of the assay and could be shortened by renewing the medium more frequently.

To assess the repercussion of the culture conditions on the intracellular cytoplasmatic levels of calcium of rMCSs cultured on CDHA, the cells were incubated with Fluo-4, a common intracellular calcium indicator dye (Figure 4) and analysed by flow cytometry [35]. The values of fluorescence per cell were normalized by the cell volume to discard differences in fluorescence associated to cell size. While the cells cultured on small discs (CDHA-S) experienced a notable increase in intracellular calcium, as observed by the higher median fluorescence value (61.87± 33.72% higher than TCPS, Figure 4B and D), there were no significant changes in intracellular calcium for the cells cultured on large discs compared to the control cells. One could hypothesize that the extracellular calcium on CDHA-S in the vicinity of the cells, may cause an increased local concentration of calcium in the fluid nearby the CDHA surface, which, by the influx through voltage gated Ca^{2+} channels [36] could lead to the increase of cytosolic Ca^{2+} values detected in the case of CDHA-S. However, for CDHA-L, the lower extracellular calcium concentration did not seem to influence intracellular calcium concentration. This later finding was surprising as we were expecting in fact an efflux of Ca from the cells to counterbalance the lower calcium content in the culture medium.

Both, extra and intracellular calcium are known to play a major role in the regulation of a number of cellular and molecular interactions [37–39]. In particular, the extracellular Ca^{2+} regulates cell spreading by stabilizing integrin structure and modulating integrin-ligand binding

[40,41]. For instance, the removal of divalent cations by EDTA (ethylenediaminetetraacetic acid) completely inhibits integrin-ligand binding [42]. Herein, we analysed the levels of pFAK as an indicator of the maturation of cellular adhesion complexes (Figure 7). When FAK is phosphorylated, it activates downstream signalling pathways that regulate, thorough polymerization of the actin cytoskeleton, not only cell adhesion and spreading but also cell proliferation, motility and survival [43]. Cells on CDHA-L developed few actin stress fibers and low pFAK levels (Figures 7A and D), which can be associated to the decreased extracellular Ca^{2+}, which can be the cause of the dramatic decrease in the number of cells (Figure 5E). Moreover, the reduction of rMSCs number on CDHA-L was accompanied with cell shrinkage (Figures 3B and 7D) and retraction of filopodia (Figures 3A and 7A). This may point to apoptotic condition of rMSCs where general rounding up of cells occurs [38,44].

For CDHA-S, when the depletion of Ca^{2+} from the cell culture medium was prevented, higher pFAK levels (Figures 7A and D) and more extensive cell spreading (Figures 3A and B; 7A and B) were observed.

In agreement with the previous results, FACS analysis showed that the number of apoptotic cells was higher on CDHA-L (Figure 5). Both immature focal adhesions and decreased intracellular/extracellular Ca^{2+} might be responsible of increased apoptosis on that condition [45], whereas on CDHA-S apoptosis levels were smaller. The involvement of the calcium ion on cellular fate has been extensively studied. For instance, most cell death pathways are triggered either through calcium signalling or through Ca^{2+} alterations at intracellular and extracellular level [37]. According to Zhivotovsky *et al.* the calcium ion regulates both necrosis and apoptosis processes [38]. Whilst necrosis occurs predominantly due to the overload of intracellular calcium, apoptosis can be triggered by more subtle changes. In this regard, apoptotic pathways can be induced either through alterations of calcium homeostasis in intracellular compartments or through Ca^{2+} - mobilised signals that activate apoptotic death effectors- mainly enzymes such as Caspases [45]. We hypothesise that reduced values of extracellular calcium might be one of the possible reasons causing the rMCSs apoptosis due to

detachment from CDHA-L substrate (Figure 4A). The FAK localization and phosphorylation in focal adhesions is required for generation of fibrillar adhesions and consequent organization of cell matrix and distribution of actin stress fibers [46]. Here, the little maturation of FAK on CDHA-L, in comparison to TCPS, is likely reflected into insufficient cell adhesion followed by their rounding up, detachment and finally death through apoptosis.

The increased cell survival on CDHA small discs allowed us to compare its osteogenic potential with that of β-TCP (Figure 8). Differentiation of rMSCs into the osteoblastic lineage was analysed by RT-qPCR. Alkaline phosphatase (ALP) and collagen I (COLL I) are markers commonly used to evaluate osteoblastic differentiation [47]. ALP expression was higher in CDHA-S compared to β-TCP-S at initial stages of cell culture, whereas COLL I was higher in β-TCP at 3 days. Osteocalcin (OCN), osteonectin (ONN) and osteopontin (OPN) are bone-specific extracellular proteins responsible of the size and quality of mineral growth as well as the regular formation of crystals [48]. Their expression was also higher on CDHA-S compared to β-TCP-S indicating a higher commitment to the osteoblastic lineage. High levels of BMP-2, a growth factor with essential roles in guiding MSCs differentiation and bone regeneration expression were observed also on CDHA-S [49]. Similar trends were observed in other studies on biomimetic calcium phosphates, suggesting a synergistic effect of surface chemistry and topography which fosters the osteogenic differentiation of osteoblasts [50,51] and MSC [6]. Moreover, in line with the increased intracellular calcium found in the cells cultured on CDHA-S, although intracellular calcium is thought to play a more significant role in osteoblast proliferation than in differentiation [36], some studies reported a correlation between intracellular calcium and the expression of osteogenic genes in osteoblasts [36] and MSCs [52]. Specifically, Barradas *et al.* reported a strong involvement of Ca^{2+} internalization in the overexpression of osteogenesis-related genes, especially BMP-2, but also other calcium-responsive genes such as OPN and OCN [11].

5. CONCLUSIONS

The results obtained in this work put forward the complexity of performing static cell culture studies on highly reactive materials such as biomimetic CDHA, due to the drastic ionic changes caused in the cell culture, associated to the continuous compositional changes that the apatitic material undergoes with incubation time. The strategy of increasing the medium/biomaterial volume ratio has proved successful in mitigating ionic exchanges and has allowed to decouple the contribution of topography from the material's reactivity on cells and has revealed the effect of ionic exchanges on rMSCs adhesion and proliferation, as well as cell morphology. Nevertheless, further studies are needed to better understand the interaction between the material and the fluid environment, being especially relevant the effect of the cell culture concentration gradients on cell response.

6. ACKNOWLEDGMENTS

The authors acknowledge the Spanish Government for financial support through MAT2015-65601-R project, co-funded by the EU through European Regional Development Funds, and FPI scholarship of JMS. They also thank the Generalitat the Catalunya for funding through project 2017SGR-1165. MPG acknowledges the ICREA Academia award by the Generalitat de Catalunya. The authors thank Montserrat Domínguez for her technical support with XPS measurements.

REFERENCES

[1] V.P. Galván-Chacón, P. Habibovic, Deconvoluting the Bioactivity of Calcium Phosphate-Based Bone Graft Substitutes: Strategies to Understand the Role of Individual Material Properties, Adv. Healthc. Mater. 6 (2017) 1–15.

[2] H. Yuan, M. Van Den Doel, S. Li, C.A. Van Blitterswijk, K. De Groot, J.D. De Bruijn, A comparison of the osteoinductive potential of two calcium phosphate ceramics implanted intramuscularly in goats, J. Mater. Sci. Mater. Med. 13 (2002) 1271–1275.

[3] C. Wang, Y. Duan, B. Markovic, J. Barbara, C. Rolfe Howlett, X. Zhang, H. Zreiqat, Proliferation and bone-related gene expression of osteoblasts grown on hydroxyapatite ceramics sintered at different temperature, Biomaterials. 25 (2004) 2949–2956.

[4] G. Muralithran, S. Ramesh, The effects of sintering temperature on the properties of hydroxyapatite, Ceram. Int. 26 (2000) 221–230.

[5] S. Samavedi, A.R. Whittington, A.S. Goldstein, Calcium phosphate ceramics in bone tissue engineering: a review of properties and their influence on cell behavior, Acta Biomater. 9 (2013) 8037–8045.

[6] C. Danoux, L. Sun, G. Koçer, Z.T. Birgani, D. Barata, J. Barralet, C. Van Blitterswijk, R. Truckenmüller, P. Habibovic, Development of Highly Functional Biomaterials by Decoupling and Recombining Material Properties, Adv. Mater. 28 (2016) 1803–1808.

[7] M. Vallet Regi, Calcium phosphates as substitution of bone tissues, Prog. Solid State Chem. 32 (2004) 1–31.

[8] R.Z. LeGeros, Calcium phosphate-based osteoinductive materials, Chem. Rev. 108 (2008) 4742–4753.

[9] A.M.C. Barradas, H. Yuan, C.A. van Blitterswijk, P. Habibovic, Osteoinductive biomaterials: current knowledge of properties, experimental models and biological mechanisms, Eur. Cell. Mater. 21 (2011) 407–429.

[10] C.B.S.S. Danoux, D.C. Bassett, Z. Othman, A.I. Rodrigues, R.L. Reis, J.E. Barralet, C.A. Van Blitterswijk, P. Habibovic, Elucidating the individual effects of calcium and phosphate ions on hMSCs by using composite materials, Acta Biomater. 17 (2015) 1–15.

[11] A.M.C. Barradas, H.A.M. Fernandes, N. Groen, Y.C. Chai, J. Schrooten, J. van de Peppel, J.P.T.M. van Leeuwen, C.A. van Blitterswijk, J. de Boer, A calcium-induced signaling cascade leading to osteogenic differentiation of human bone marrow-derived mesenchymal stromal cells., Biomaterials. 33 (2012) 3205–15.

[12] J. Gustavsson, M.P. Ginebra, E. Engel, J. Planell, Ion reactivity of calcium-deficient hydroxyapatite in standard cell culture media, Acta Biomater. 7 (2011) 4242-4252.

[13] J. Gustavsson, M.P. Ginebra, J. Planell, E. Engel, Osteoblast-like cellular response to dynamic changes in the ionic extracellular environment produced by calcium-deficient hydroxyapatite., J. Mater. Sci. Mater. Med. 23 (2012) 2509–2520.

[14] K. Klimek, A. Belcarz, R. Pazik, P. Sobierajska, T. Han, R.J. Wiglusz, G. Ginalska, "false" cytotoxicity of ions-adsorbing hydroxyapatite - Corrected method of cytotoxicity evaluation for ceramics of high specific surface area, Mater. Sci. Eng. C. 65 (2016) 70–79.

[15] M.P. Ginebra, E. Fernández, E.A.P. De Maeyer, R.M.H. Verbeeck, M.G. Boltong, J. Ginebra, F.C.M. Driessens, J. A. Planell, Setting reaction and hardening of an apatitic calcium phosphate cement., J. Dent. Res. 76 (1997) 905–912.

[16] J.-M. Sadowska, J. Guillem-Marti, E.B. Montufar, M. Espanol, M.-P. Ginebra, Biomimetic Versus Sintered Calcium Phosphates: The In Vitro Behavior of Osteoblasts and Mesenchymal Stem Cells, Tissue Eng. Part A. 23 (2017) 1297–1309.

[17] A. Barba, A. Diez-Escudero, Y. Maazouz, K. Rappe, M. Espanol, E.B. Montufar, M. Bonany, J.M. Sadowska, J. Guillem-Marti, C. Öhman-Mägi, C. Persson, M.C. Manzanares, J. Franch, M.P. Ginebra, Osteoinduction by Foamed and 3D-Printed Calcium Phosphate Scaffolds: Effect of Nanostructure and Pore Architecture, ACS Appl. Mater. Interfaces. 9 (2017) 41722–41736.

[18] J. Stern, W.H.P. Lewis, The colorimetric estimation of calcium in serum with o-cresolphthalein complexone, Clin. Chim. Acta. 2 (1957) 576–580.

[19] J. Gitelman, An Improved Automated Procedure of Calcium in Biological for the Determination Specimens, Anal. Biochem. 18 (1967) 521–531.

[20] M.W. Pfaffl, A new mathematical model for relative quantification in real-time RT-PCR, Nucleic Acids Res. 29 (2001) 45e–45.

[21] M.E. Fleet, Infrared spectra of carbonate apatites: ν2-Region bands, Biomaterials. 30 (2009) 1473–1481.

[22] R. Murugan, S. Ramakrishna, Production of ultra-fine bioresorbable carbonated hydroxyapatite, Acta Biomater. 2 (2006) 201–206.

[23] W. Bonfield, I.R. Gibson, Novel synthesis and characterization of an AB-type carbonate-substituted hydroxyapatite, J. Biomed. Mater. Res. 59 (2002) 697–708.

[24] C. Rey, B. Collins, T. Goehl, I.R. Dickson, M.J. Glimcher, The carbonate environment in bone mineral: A resolution-enhanced fourier transform infrared spectroscopy study, Calcif. Tissue Int. 45 (1989) 157–164.

[25] M.S. Sader, K. Lewis, G.A. Soares, R.Z. LeGeros, Simultaneous incorporation of magnesium and carbonate in apatite: effect on physico-chemical properties, Mater. Res. 16 (2013) 779–784.

[26] S. Padilla, I. Izquierdo-Barba, M. Vallet-Regi, High specific surface area in nanometric carbonated hydroxyapatite, Chem. Mater. 20 (2008) 5942–5944.

[27] A. Vines, G.J. McBean, A. Blanco-Fernández, A flow-cytometric method for continuous measurement of intracellular Ca^{2+} concentration, Cytom. Part A. 77 (2010) 1091–1097.

[28] A.D. Posey, O.U. Kawalekar, C.H. June, Measurement of Intracellular Ions by Flow Cytometry, Curr. Protoc. Cytom. 2015 (2015) 9.8.1-9.8.21.

[29] H. Yuan, H. Fernandes, P. Habibovic, J. de Boer, A.M.C. Barradas, A. de Ruiter, W.R. Walsh, C.A. van Blitterswijk, J.D. de Bruijn, Osteoinductive ceramics as a synthetic alternative to autologous bone grafting., Proc. Natl. Acad. Sci. U. S. A. 107 (2010) 13614–13619.

[30] A.M.C. Barradas, H. Yuan, J. van der Stok, B. Le Quang, H. Fernandes, A. Chaterjea, M.C.H. Hogenes, K. Shultz, L.R. Donahue, C. van Blitterswijk, J. de Boer, The influence of genetic factors on the osteoinductive potential of calcium phosphate ceramics in mice, Biomaterials. 33 (2012) 5696–5705.

[31] Y.K. Liu, Q.Z. Lu, R. Pei, H.J. Ji, G.S. Zhou, X.L. Zhao, R.K. Tang, M. Zhang, The effect of extracellular calcium and inorganic phosphate on the growth and osteogenic differentiation of mesenchymal stem cells in vitro: implication for bone tissue engineering, Biomed. Mater. 4 (2009) 025004

[32] A. Diez-Escudero, M. Espanol, S. Beats, M.-P. Ginebra, In vitro degradation of calcium phosphates: Effect of multiscale porosity, textural properties and composition, Acta Biomater. 60 (2017) 81–92.

[33] P. Gao, H. Zhang, Y. Liu, B. Fan, X. Li, X. Xiao, P. Lan, M. Li, L. Geng, D. Liu, Y. Yuan, Q. Lian, J. Lu, Z. Guo, Z. Wang, Beta-tricalcium phosphate granules improve osteogenesis in vitro and establish innovative osteo-regenerators for bone tissue engineering in vivo, Sci. Rep. 6 (2016) 1–14.

[34] Y. Liu, Y. Ma, J. Zhang, Q. Xie, Z. Wang, S. Yu, Y. Yuan, C. Liu, MBG-Modified β-TCP Scaffold Promotes Mesenchymal Stem Cells Adhesion and Osteogenic Differentiation via a FAK/MAPK Signaling Pathway, ACS Appl. Mater. Interfaces. 9 (2017) 30283–30296.

[35] K.R. Gee, K.A. Brown, W.N. Chen, J. Bishop-Stewart, D. Gray, I. Johnson, Chemical and physiological characterization of fluo-4 Ca(2+)-indicator dyes, Cell Calcium. 27 (2000) 97–106.

[36] M. Zayzafoon, Calcium/calmodulin signaling controls osteoblast growth and differentiation, J. Cell. Biochem. 97 (2006) 56–70.

[37] M.J. Berridge, P. Lipp, M.D. Bootman, The versatility and universality of calcium signalling, Nat. Rev. Mol. Cell Biol. 1 (2000) 11–21.

[38] B. Zhivotovsky, S. Orrenius, Calcium and cell death mechanisms: A perspective from the cell death community, Cell Calcium. 50 (2011) 211–221.

[39] S. Sun, Y. Liu, S. Lipsky, M. Cho, Physical manipulation of calcium oscillations facilitates osteodifferentiation of human mesenchymal stem cells, FASEB J. 21 (2007) 1472–1480.

[40] K. Zhang, J. Chen, The regulation of integrin function by divalent cations, Cell Adhesion & Migration. 6 (2012) 20-29.

[41] J. Xiong, T. Stehle, S.L. Goodman, M.A. Arnaout, Integrins, cations and ligands: making the connection. Journal of Thrombosis and Haemostasis, 1 (2003) 1642-1654..

[42] A.P. Mould, A.N. Garratt, W. Puzon-McLaughlin, Y. Takada, M.J. Humphries, Regulation of integrin function: evidence that bivalent-cation-induced conformational changes lead to the unmasking of ligand-binding sites within integrin alpha5 beta1. Biochem J. 331 (Pt 3) (1998) 821-8.

[43] J.T. Parsons, Focal adhesion kinase: the first ten years, J. Cell Sci. 116 (2003) 1409–1416.

[44] G. Kroemer, L. Galluzzi, P. Vandenabeele, J. Abrams, E.S. Alnemri, E.H. Baehrecke, M. V Blagosklonny, W.S. El-Deiry, P. Golstein, D.R. Green, M. Hengartner, R. a Knight, S. Kumar, S. a Lipton, W. Malorni, G. Nuñez, M.E. Peter, J. Tschopp, J. Yuan, M. Piacentini, B. Zhivotovsky, G. Melino, Classification of cell death: recommendations of the Nomenclature Committee on Cell Death 2009., Cell Death Differ. 16 (2009) 3–11

[45] S. Orrenius, B. Zhivotovsky, P. Nicotera, Calcium: Regulation of cell death: the calcium–apoptosis link, Nat. Rev. Mol. Cell Biol. 4 (2003) 552–565.

[46] D. Ilić, B. Kovacic, K. Johkura, D.D. Schlaepfer, N. Tomasević, Q. Han, J.-B. Kim, K. Howerton, C. Baumbusch, N. Ogiwara, D.N. Streblow, J. a Nelson, P. Dazin, Y. Shino, K. Sasaki, C.H. Damsky, FAK promotes organization of fibronectin matrix and fibrillar adhesions, J. Cell Sci. 117 (2004) 177–187.

[47] E.E. Golub, G. Harrison, a G. Taylor, S. Camper, I.M. Shapiro, The role of alkaline phosphatase in cartilage mineralization, Bone Miner. 17 (1992) 273–278.

[48] H.I. Roach, Why does bone matrix contain non-collagenous proteins? The possible roles of osteocalcin, osteonectin, osteopontin and bone sialoprotein in bone mineralisation and resorption, Cell Biol. Int. 18 (1994) 617–628.

[49] V. Rosen, BMP2 signaling in bone development and repair, Cytokine Growth Factor Rev. 20 (2009) 475–480.

[50] R. Shu, R. McMullen, M.J. Baumann, L.R. McCabe, Hydroxyapatite accelerates differentiation and suppresses growth of MC3T3-E1 osteoblasts, J. Biomed. Mater. Res. A. 67 (2003) 1196–1204.

[51] S. Sethuraman, L.S. Nair, S. El-Amin, M.-T.N. Nguyen, Y.E. Greish, J.D. Bender, P.W. Brown, H.R. Allcock, C.T. Laurencin, Novel low temperature setting nanocrystalline calcium phosphate cements for bone repair: Osteoblast cellular response and gene expression studies, J. Biomed. Mater. Res. Part A. 82A (2007) 884–891.

[52] L. Petecchia, F. Sbrana, R. Utzeri, M. Vercellino, C. Usai, L. Visai, M. Vassalli, P. Gavazzo, Electro-magnetic field promotes osteogenic differentiation of BM-hMSCs through a selective action on Ca^{2+} -related mechanisms, Sci. Rep. 5 (2015) 1–13.

FIGURE LEGENDS

Figure 1. A) Scanning electron microscopy (left panel) and optical interferometry (right panel) images of CDHA and β-TCP substrates. Scale bar denotes 40 μm in the main images and 2 μm in the insets with magnified micrographs; B) Scheme of cell culture experiment.

Figure 2. A) Proliferation of rMSCs at 6 hours, 3, 7 and 14 days. Bars represent means ± SD of three experiments. * indicates significant differences ($p<0.05$) between CDHA- L and CDHA- S at each time point. & indicates significant differences ($p<0.05$) between β-TCP- L and β-TCP- S at each time point. # indicates significant differences ($p<0.05$) compared with TCPS at each time point; B) upper panel: Concentration of Ca^{2+} in the supernatants at 6 hours, 3, 7 and 14 day of cell culture; middle panel: Concentration of P_i in the supernatants at 6 hours, 3, 7 and 14 day of cell culture; bottom panel: pH of the supernatants at 6 hours, 3, 7 and 14 day of cell culture. The evaluation of ionic composition and pH of supernatants was performed in presence of cells. C) The effect of FBS-free advDMEM medium on CDHA chemistry; left: The Ca/P ratio of CDHA-L and CDHA-S discs after 0, 14 and 21 days of incubation with culture media; right: The ATR- FTIR spectra of CDHA-L surface. The evaluation of CDHA-L and CDHA-S substrates was performed without presence of cells in culture medium. * indicates significant differences ($p<0.05$) between CDHA- L and CDHA- S at each time point. . Letters (a,b) identify differences ($p<0.05$) between the time points within the same sample.

Figure 3. A) Morphology of rMSCs observed by SEM on CDHA-L, CDHA-S, β-TCP-L and β-TCP-S at 6 hours, 3, 7 and 14 days. To better distinguish rMSCs on CDHA-L, some cells are labelled with white arrows. Scale bar denotes 100 μm; B) cell spreading and C) aspect ratio on CaPs substrates over cell culture. Symbols represent individual cells (n=15), the boxes represent 25^{th} and 75^{th} percentile, the middle line is the median and whiskers are standard deviation. n.p.- not provided: due to the high density of cells on β-TCP-L and β-TCP-S at day 14, the quantification of morphological features of rMSCs was precluded. * indicates significant differences ($p<0.05$) between L (CDHA-L and β-TCP-L) and S (CDHA-L and β-TCP-L) substrates at each time point; a indicates significant differences ($p<0.05$) compared with 6h for each sample. No other statistically significant differences were detected.

Figure 4. Flow cytometric analysis of intracellular calcium of CDHA-L, CDHA-S and control at 6 hours. A) The dot plots show the gate (coloured dots) of viable cells that was set for analysis of Fluo-4 fluorescence; B) Histograms of fluorescence of Fluo-4 normalised versus

forward scatter (cell size); C) Histograms of cell size (forward scatter); D) Mean± standard error of median fluorescence of Fluo-4 from three independent runs. The median fluorescence for CDHA-L and CDHA-S was represented as a percentage of median fluorescence of the control (TCPS) establishing that it is equal to 100% (that is why the error bar for control group is not visible on the plot). * and # indicates groups with significant differences ($p < 0.05$).

Figure 5. A), B) and C) apoptosis/ necrosis assay by flow cytometry. Cells positively stained for Alexa Fluor 488 annexin V and negatively for PI were considered as apoptotic. Cells positively stained for both Alexa Fluor 488 annexin V and PI were considered as late apoptotic. Cells negatively stained for Alexa Fluor 488 annexin V and positively for PI are considered necrotic. The percentage of each population of cells is presented in corresponding square of each graph; D), E) and F): Representative confocal images of rMSCs stained for apoptosis (green)/ necrosis (red) with annexin V/ PI and nuclei (blue) (merged); G), H) and I): Representative confocal images of rMSCs stained for apoptosis (green). Scale bar denotes 100 µm. The brightness and contrast of images was adjusted using Fiji/Image-J package.

Figure 6. Merged images of rMSCs stained for F-actin (red), nuclei (blue) and fibronectin (green) on CDHA-L (A, B, C, D), CDHA-S (E, F, G, H) and control i.e glass coverslips (I, J, K, L) at 6 hours, 1, 2 and 3 days of cell culture respectively. Scale bar denotes 100 µm.

Figure 7. A) Merged images of cells stained for F-actin (red), nuclei (blue) and pFAK (green) on CDHA-L, CDHA-S, and control i.e glass coverslips at 6 hours, 1, 2 and 3 days of cell culture. The last column shows the pFAK/ DAPI staining of rMSCs on CDHA-L, CDHA-S and control, at day 3. pFAK was indicated with white arrows. Scale bar denotes 40 µm. The brightness and contrast of images was adjusted using Fiji/Image-J package. B) and C), respectively: Evolution of spreading and aspect ratio of cells on CDHA-L and CDHA-S at the different time points; D) Area of pFAK at day 3 of cell culture. Symbols represent individual cells (n=15 in B) and C) and n=10 in D), the boxes represent 25^{th} and 75^{th} percentile, the middle

line is the median and whiskers are standard deviation. * indicates significant differences ($p<0.05$) between CDHA substrates at each specific time point. # indicates significant difference ($p<0.05$) compared with control at each time point. Letters (a,b,c) identify differences ($p<0.05$) between the time points within the same sample.

Figure 8. ALP, COLL I, OCN, ONN, OPN and BMP-2 gene expression of rMSCs cultured on CDHA-S and β-TCP-S. Expression levels were determined by quantitative real time RT-PCR, normalised versus TCPS at 6 hours and displayed relative to their housekeeping gene. Bars represent mean ± SE of three experiments. * indicates significant difference between substrates at the same time point ($p<0.05$). The patterned bars indicate the usage of osteogenic medium.

SUPPLEMENTARY INFORMATION

Supplementary Figure 1. XRD patterns of CDHA and β-TCP. The phase composition of the CaP substrates was determined by X-ray diffraction (XRD; D8 Advance; Bruker, Karlsruhe, Germany). The diffractometer equipped with a Cu Ka X-ray tube was operated at 40 kV and 40 mA. Data were collected in 0.02ºsteps over the 2θ range of 10–60º, with a counting time of 2 s per step. The diffraction patterns were compared to the Joint Committee on Powder Diffraction Standards for HA (JCPDS 82-1943) and β-TCP (JCPDS 70-2065)."

Supplementary Figure 2. The effect of cell culture medium on surface topography of CDHA. The evaluation was performed without presence of cells in culture medium. The samples were incubated with FBS-free advDMEM. After exposure to culture medium, the surface of CDHA-L and CDHA-S was observed through SEM. The substrates exposed to cell culture medium for 14 and 21 days exhibited similar plate- like morphology compared to pristine CDHA.

Supplementary Figure 3. The effect of cell culture medium on surface composition of CDHA. . The evaluation was performed without presence of cells in culture medium. The samples were

incubated with FBS-free advDMEM. The surface chemistry of CDHA-L and CDHA-S was determined through X-ray photoelectron spectroscopy (XPS). An area of 2 mm x 3 mm of one sample (n=1) was subjected to XPS analysis and ten measurements were performed. The relative error associated to the survey spectra XPS measurements was of 0.5%.The spectra were acquired in ultrahigh vacuum (5×10^{-9} mbar) with an XR50 Mg anode source operating at 150 W and a Phoibos 150 MCD-9 detector (D8 advance, SPECS Surface Nano Analysis GmbH, Germany). The spectra for C 1s, O 1s, Ca 2p, P 2p and Mg 2p were recorded at pass energy of 25 eV with step size of 0.1 eV. The CasaXPS software (Casa Software Ltd, UK) was used for the determination of atomic elemental composition using C 1s peak as a reference. A) XPS spectra of CDHA-L (left) and CDHA-S (right) after 0, 14 and 21 days of incubation with cell culture media. B) The superficial Ca/P ratio of CDHA-L and CDHA-S discs after 0, 14 and 21 days of incubation with culture media. The superficial Ca/P ratio of CDHA-L and CDHA-A increased after exposure to cell culture media. C) Concentration of Ca^{2+} in the supernatants at 6 hours, 3, 7 and 14 and 21 day evaluated through o- cresolphthalein complexone method. The CDHA-S maintained similar calcium levels to those observed in TCPS. The depletion of Ca^{2+} for CDHA-L substrate was more pronounced in FBS- free advDMEM than the decrease of calcium observed for CDHA-L incubated with cells and complete advDMEM (Figure 2B).

Supplementary Figure 4. The Mg/P ratio (A) and Na/P ratio (B) of CDHA-L and CDHA-S discs after 0, 14 and 21 days of incubation with culture media evaluated through ICP-MS. The evaluation was performed without presence of cells in culture medium. The samples were incubated with FBS-free advDMEM. The incubation with cell culture medium led to an increase of the Mg/P and Na/P ratio for both CDHA-L and CDHA-S. Overall, CDHA substrates showed similar Mg/P and Na/P ratios at 14 and 21 day of incubation except for CDHA-S where Na/P ratio increased between 14 and 21 day. * indicates significant differences ($p<0.05$) between CDHA- L and CDHA- S at each time point. . Letters (a,b) identify differences ($p<0.05$) between the time points within the same sample.

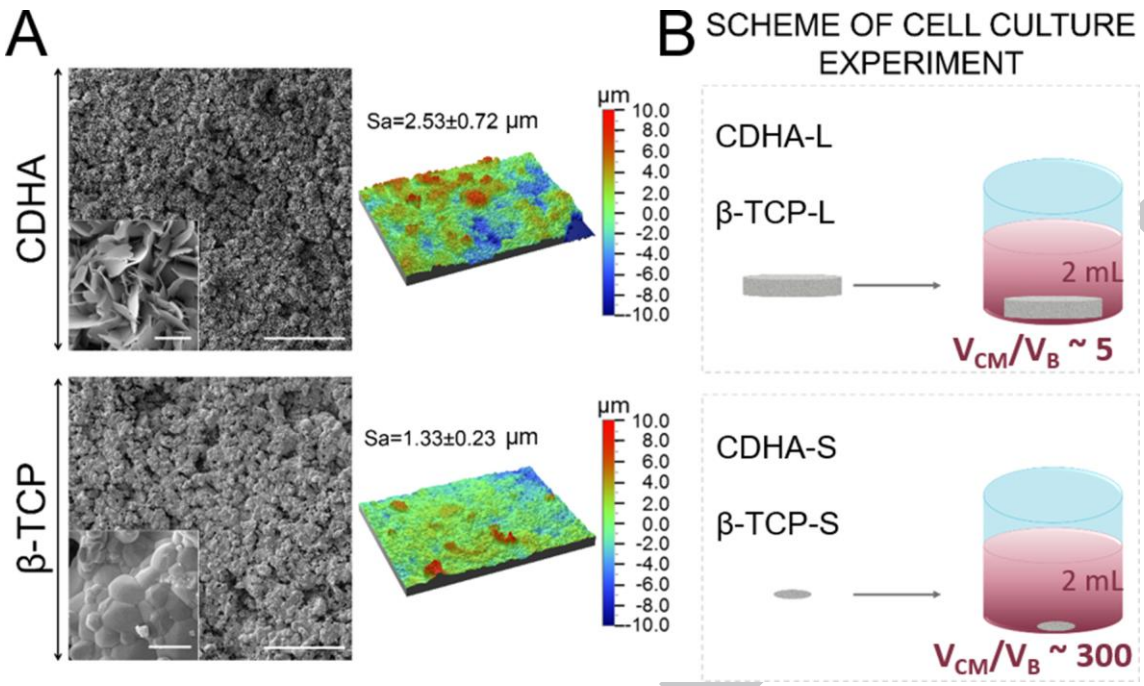

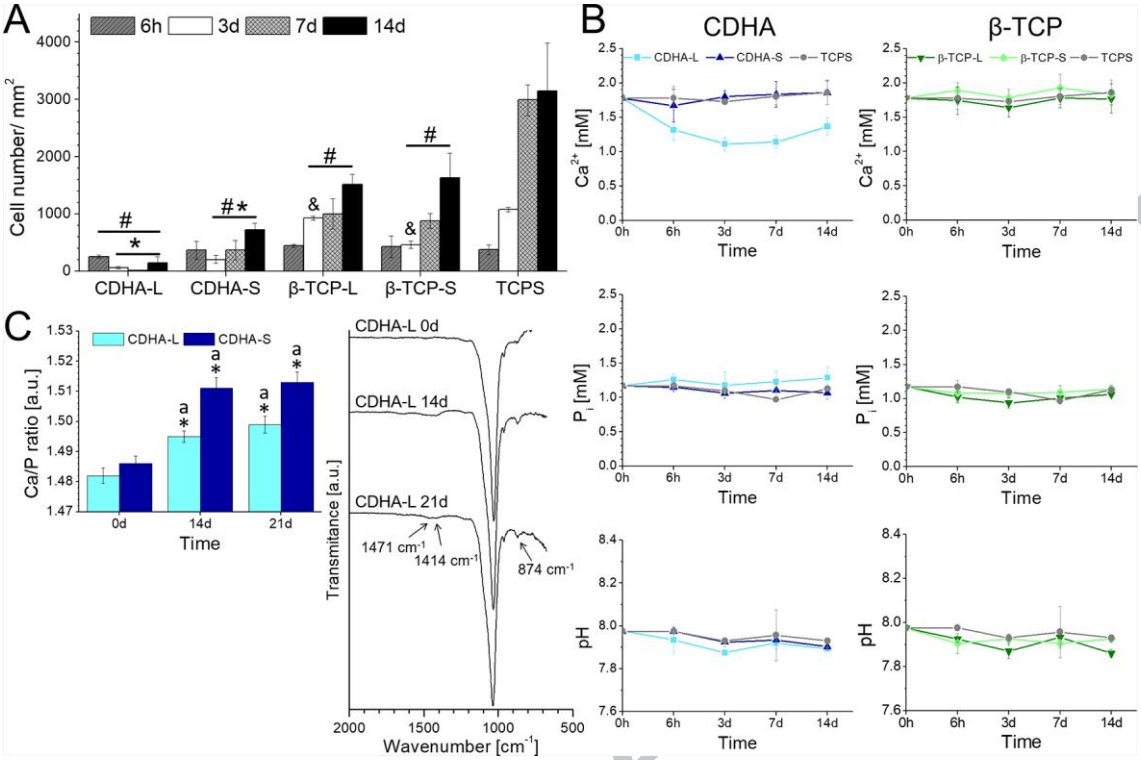

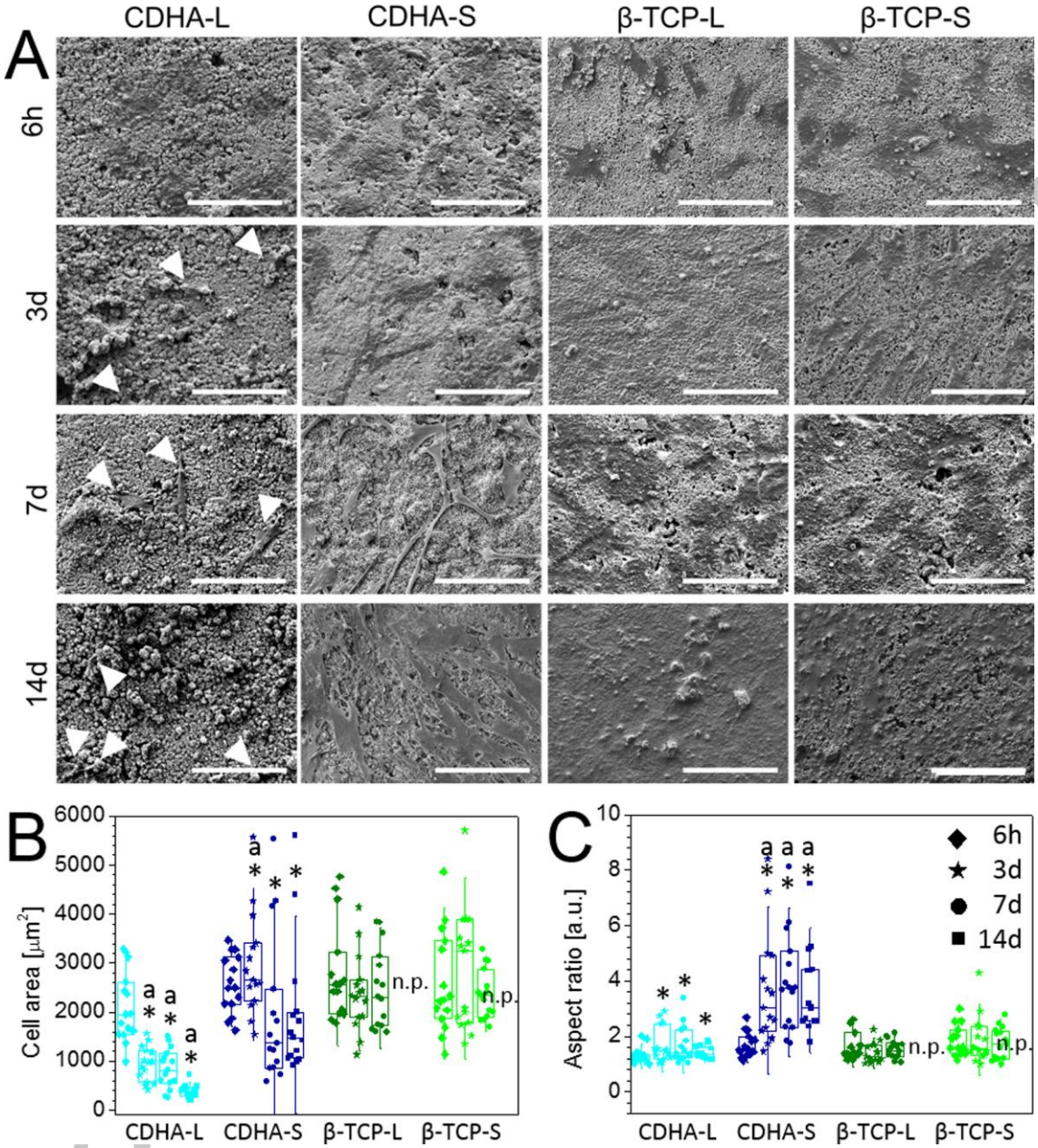
A
CDHA-L
CDHA-S
β-TCP-L
β-TCP-S
6h
3d
7d
14d
B
Cell area [μm²]
6000
5000
4000
3000
2000
1000
0
a
n.p.
CDHA-L
CDHA-S
β-TCP-L
β-TCP-S
C
Aspect ratio [a.u.]
10
8
6
4
2
0
6h
3d
7d
14d
n.p.

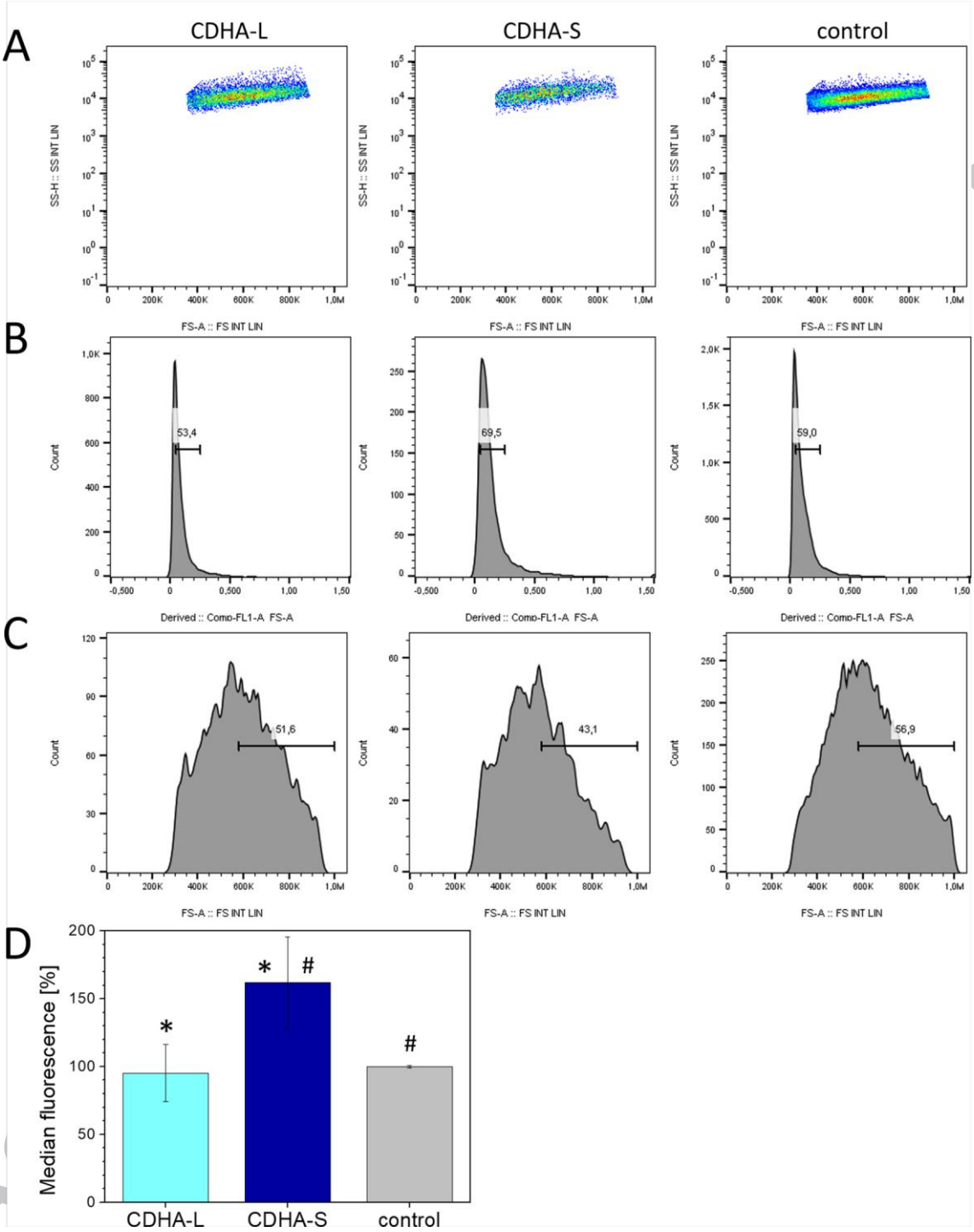

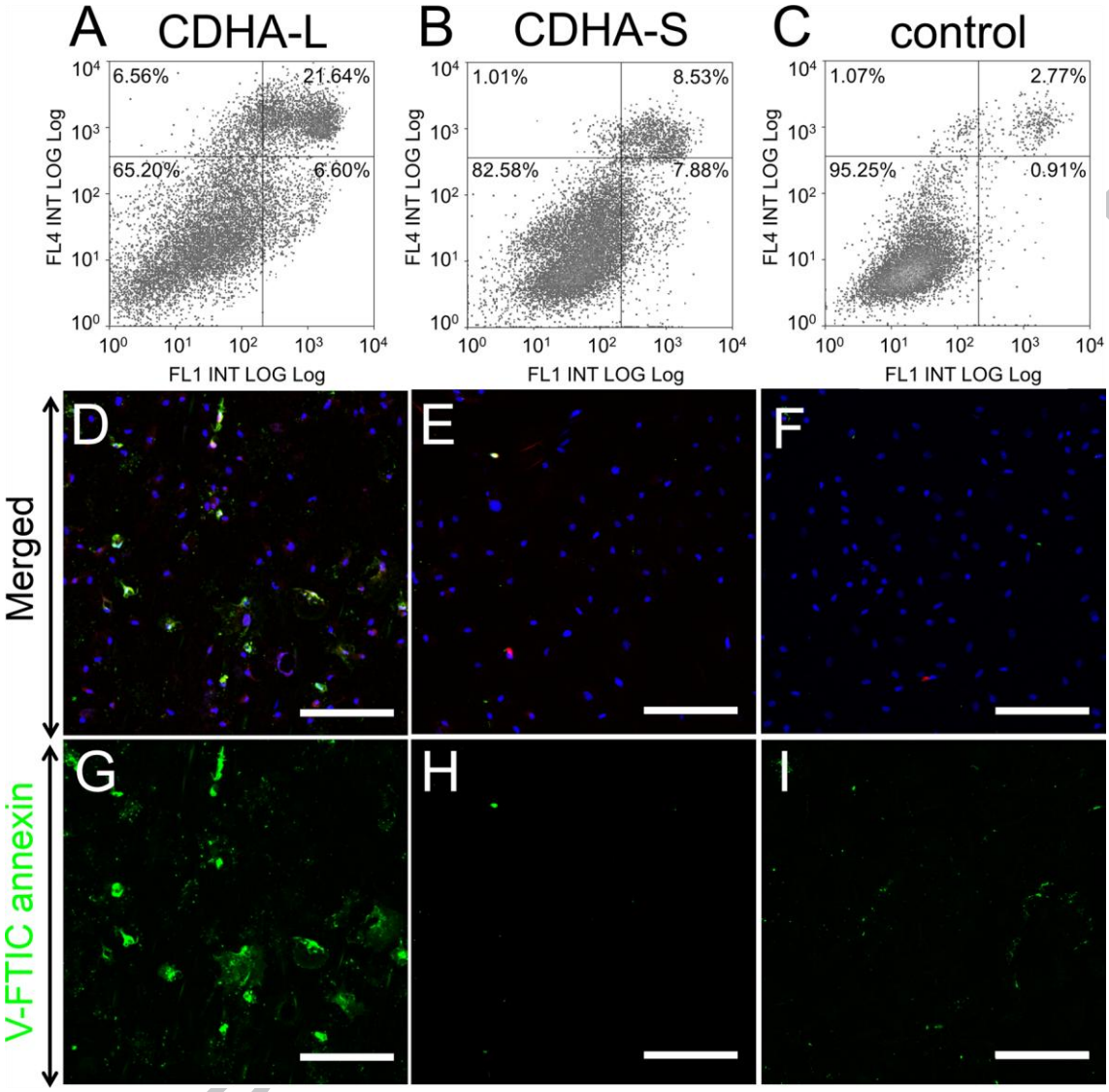
A CDHA-L
B CDHA-S
C control
6.56%
21.64%
65.20%
6.60%
1.01%
8.53%
82.58%
7.88%
1.07%
2.77%
95.25%
0.91%
FL4 INT LOG Log
FL1 INT LOG Log
Merged
V-FTIC annexin
D
E
F
G
H
I

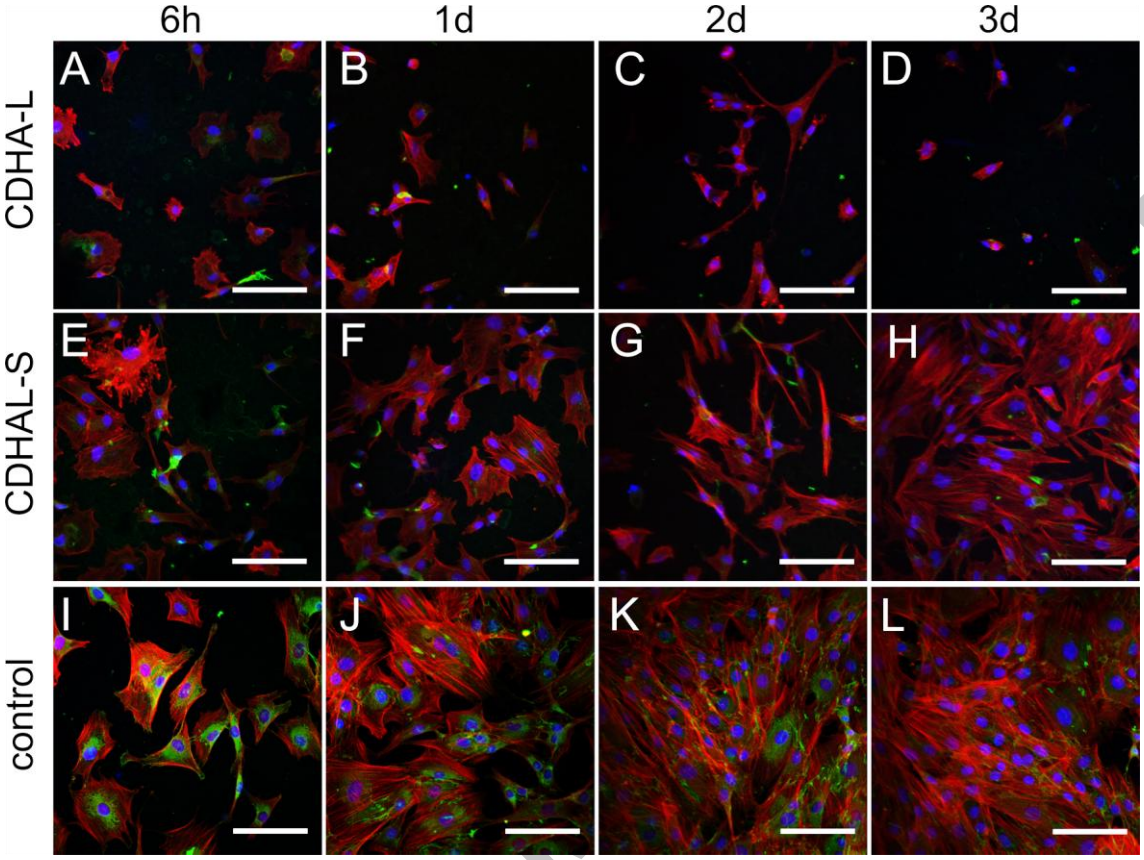

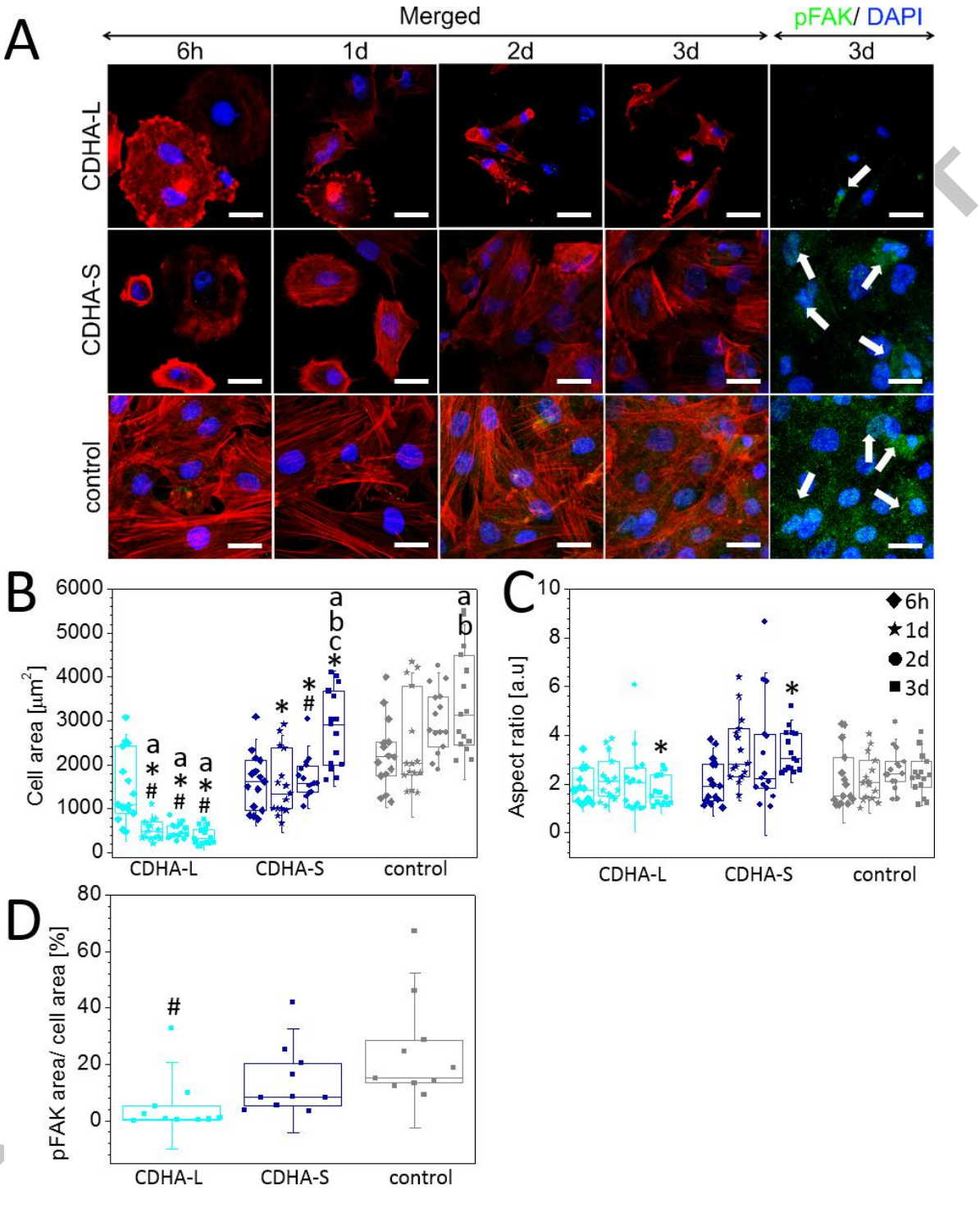
A
Merged
pFAK/ DAPI
6h
1d
2d
3d
3d
CDHA-L
CDHA-S
control
B
Cell area [μm²]
CDHA-L
CDHA-S
control
C
Aspect ratio [a.u]
6h
1d
2d
3d
CDHA-L
CDHA-S
control
D
pFAK area/ cell area [%]
CDHA-L
CDHA-S
control

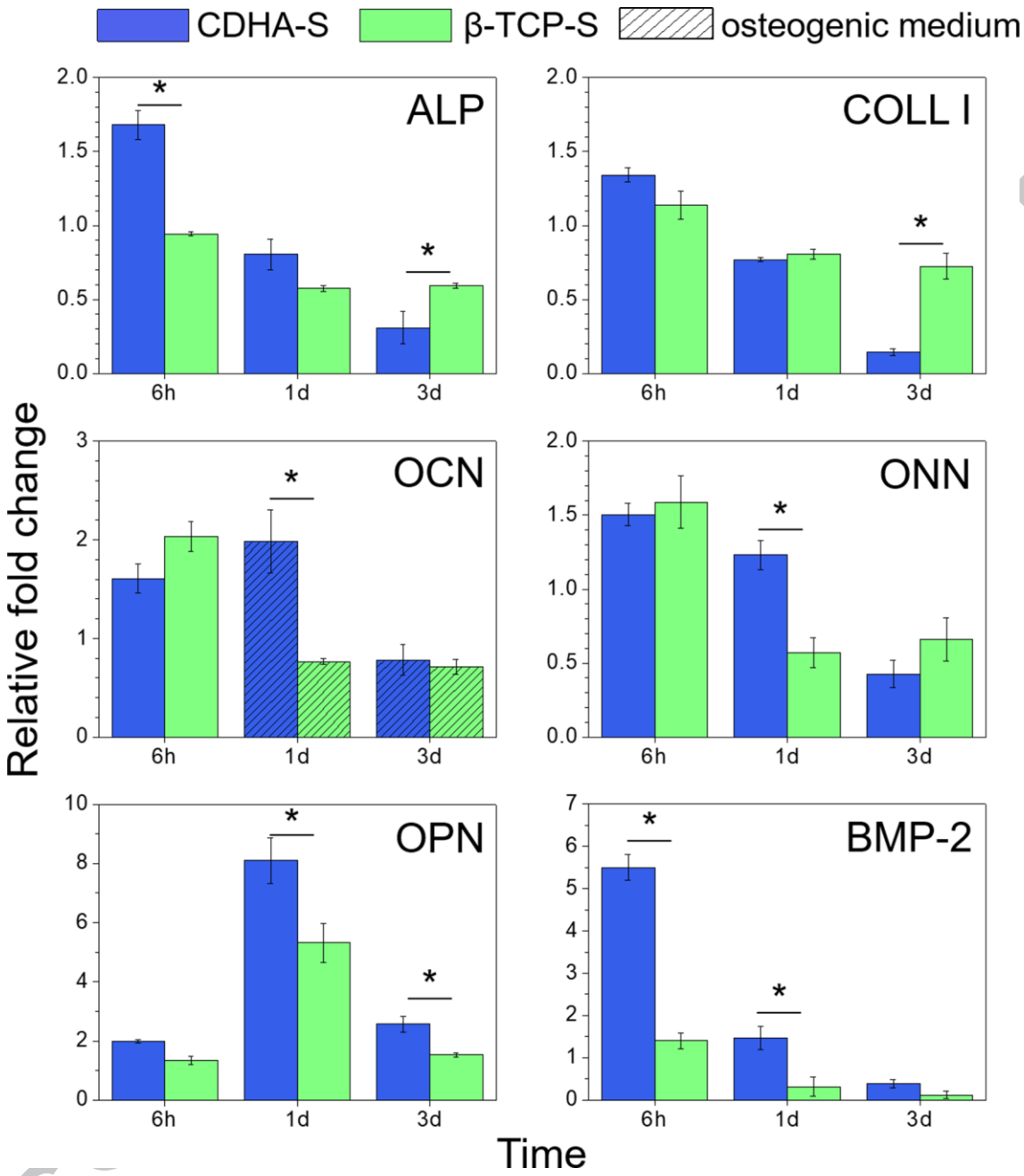
CDHA-S
β-TCP-S
osteogenic medium
ALP
COLL I
OCN
ONN
OPN
BMP-2
Relative fold change
Time
6h
1d
3d
*